The Optical Gravitational Lensing Experiment. OGLE-III Photometric Maps of the Galactic Bulge Fields*

by

M.K. Szymański[1], A. Udalski[1], I. Soszyński[1], M. Kubiak[1], G. Pietrzyński[1,2], R. Poleski[1], Ł. Wyrzykowski[3,1] and K. Ulaczyk[1]

[1] Warsaw University Observatory, Al. Ujazdowskie 4, 00-478 Warszawa, Poland
e-mail: (msz,udalski,soszynsk,mk,pietrzyn,rpoleski,kulaczyk)@astrouw.edu.pl
[2] Universidad de Concepción, Departamento de Astronomia, Casilla 160–C, Concepción, Chile
[3] Institute of Astronomy, University of Cambridge, Madingley Road, Cambridge CB3 0HA, UK
e-mail: wyrzykow@ast.cam.ac.uk

ABSTRACT

We present OGLE-III Photometric Maps of the Galactic bulge fields observed during the third phase of the OGLE project. This paper describes the last, concluding set of maps based on OGLE-III data.

The maps contain precise, calibrated *VI* photometry of about 340 million stars from 267 fields in the Galactic bulge observed during entire OGLE-III phase (2002–2009), covering about 92 square degrees in the sky. Precise astrometry of these objects is also provided.

We briefly discuss the photometry procedures and the quality of the data. We also present sample data and color–magnitude diagrams of the observed fields.

All photometric data are available to the astronomical community from the OGLE Internet archive.

1. Introduction

The Optical Gravitational Lensing Experiment (OGLE) is a long term project (started in 1992) with scientific goals including gravitational microlensing, search for extrasolar planets, variable stars etc. All these goals require regular monitoring of millions of stars in dense stellar fields located in the Galactic center, Magellanic Clouds and selected parts of the Galactic disk. The photometry of all these stars collected during the project lifetime constitutes a unique, huge data set that can be used in many astrophysical applications.

Since the second phase of the project, OGLE-II, we have published precisely calibrated, both photometrically and astrometrically, general *BVI* or *VI* catalogs of objects called OGLE Photometric Maps. These Maps cover the main project targets including the Magellanic Clouds, Galactic disk and the Galactic center.

*Based on observations obtained with the 1.3 m Warsaw telescope at the Las Campanas Observatory of the Carnegie Institution for Science.

The OGLE maps were often used, for example, for modeling the structure of the observed objects (*e.g.*, Rattenbury *et al.* 2007, Subramaniam and Subramanian 2009, Nataf *et al.* 2010), determination of the interstellar extinction (*e.g.*, Udalski *et al.* 2003b, Haschke, Grebel and Duffau 2011) or in many analyzes of microlensing events (*e.g.*, Bennett *et al.* 2010, Abe *et al.* 2004). Also, the maps constitute a huge set of the secondary photometric standards that can be used for calibration of photometry.

This paper presents the OGLE-III Photometric Map of the Galactic bulge, concluding the most recent series of the OGLE Photometric Maps which contain the photometry of objects observed during the third phase of the project. The previous papers of this series have covered the stellar fields in the Large and Small Magellanic Clouds (Udalski *et al.* 2008bc) and the Galactic disk (Szymański *et al.* 2010). The Galactic bulge photometry constitutes the biggest data set in the series, containing almost 340 million stars observed in 267 dense fields of the center of Galaxy covering 92 square degrees.

2. Observations

Observations were carried out at Las Campanas Observatory in Chile, operated by the Carnegie Institution for Science, using the 1.3-m Warsaw Telescope equipped with the eight-chip mosaic CCD camera (Udalski 2003a) covering 35×35 arcmin in the sky with the scale of 0.26 arcsec/pixel.

OGLE-III photometry of the Galactic center contains data obtained in the *V*- and *I*-band filters which are close to the standard *VI* bands. Only for very red objects, $(V-I) > 2$ mag, the data obtained through the OGLE-III glass *I* filter could not be precisely calibrated. This small deficiency has been recently fixed using calibrations based on the first OGLE-IV data, obtained with a new, 32-chip CCD camera equipped with interferometric *I*-band filter which very accurately reproduces the standard *I* pass-band. The details of this procedure will be given in Section 3.

Observations of the Galactic bulge fields consist of 89 175 exposures spanning almost eight years between June 2001 and May 2009. The vast majority of frames (87 787) were obtained in *I*-band. The remaining 1 388 frames were taken in *V* filter in order to collect some color data for the observed stars. This asymmetric strategy proved to be the most effective in terms of search for microlensing phenomena – the main scientific goal of the project – and was adopted in all phases of the experiment. The exposure times of the majority of frames were 120 s for *I*-band and 200 s for *V*-band.

The data were taken only in good seeing and transparency conditions. The seeing limit for Galactic bulge fields was set to $\approx 1\farcs8$ but it was not automatically enforced so the databases include some frames taken at worse conditions. The median seeing of the *I*-band images is equal to $1\farcs2$.

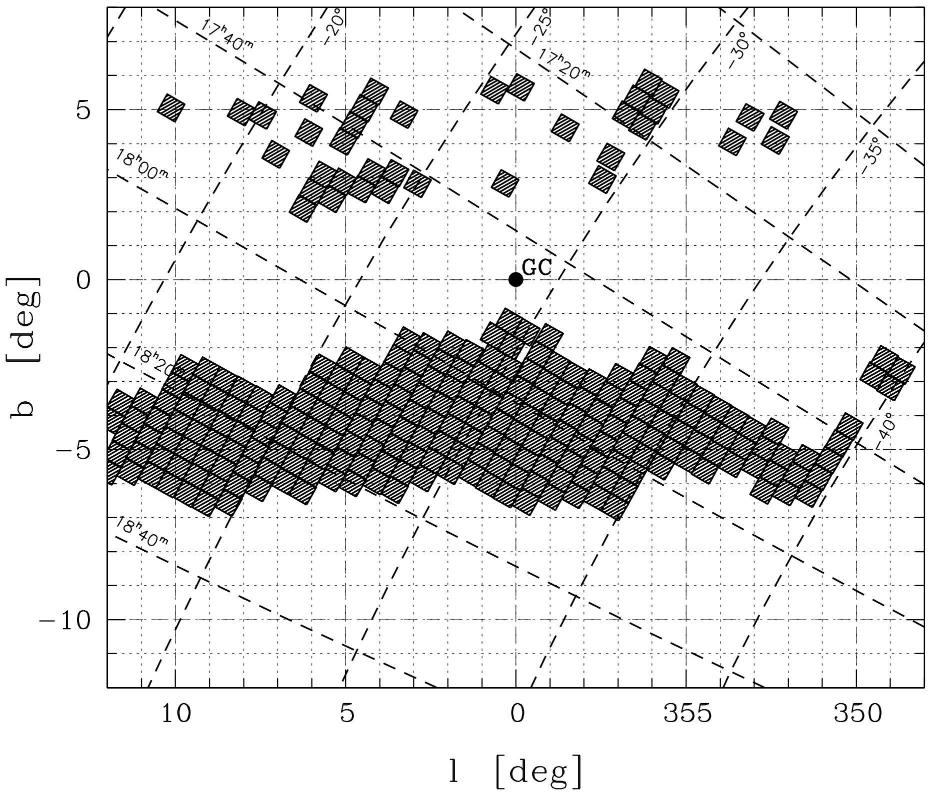

Fig. 1. Map of OGLE-III Galactic bulge fields.

Table 1 lists all Galactic bulge fields covered by the OGLE-III Photometric Maps giving their names, equatorial and galactic coordinates, number of frames (*I* and *V*) included in the databases, the number of stars detected in *I*-band and the mean value of $(V-I)$ color. Schematic map of the fields on grids of equatorial and galactic coordinates is shown in Fig. 1. The total area covered by the fields is about 92 square degrees (79 and 13 square degrees south and north of galactic equator, respectively). About 7% of this area, 6.3 square degrees, is covered by the overlapping parts of adjacent fields. This includes both overlaps of the neighboring main fields, resulting from the design of the Galactic bulge pointings (Fig. 1) and overlaps of the subfields of adjacent chips of the mosaic which are possible due to limited accuracy of telescope pointing. We used this opportunity to construct reference images which are bigger than single frames: 2180×4176 *vs.* 2048×4096 pixels per chip (see Udalski *et al.* 2008a for details), thus covering, at least partly, the gaps between CCD mosaic chips.

The number of frames taken of each field should be considered with caution. This is due to the observational strategy adopted for OGLE-III phase which allowed to switch to a much denser, sometimes even nearly continuous coverage of fields in which extremely interesting microlensing events were detected online through our early warning (EWS and EEWS) systems. For these fields, the total number of

Table 1

OGLE-III fields in Galactic bulge

Field	RA	Dec (J2000)	l_{II}	b_{II}	Nfr_I	Nfr_V	Nobj	$\langle V-I\rangle$
BLG100	$17^{h}51^{m}00.^{s}0$	$-29^\circ59'48''$	359.6961	-1.5504	2393	8	1484138	2.79
BLG101	$17^{h}53^{m}40.^{s}2$	$-29^\circ49'52''$	0.1331	-1.9643	2418	34	2269274	2.10
BLG102	$17^{h}56^{m}20.^{s}2$	$-29^\circ30'51''$	0.6991	-2.3049	2540	17	2026597	2.04
BLG103	$17^{h}56^{m}20.^{s}2$	$-30^\circ06'22''$	0.1865	-2.6018	1393	4	1858589	2.07
BLG104	$17^{h}59^{m}00.^{s}3$	$-29^\circ28'17''$	1.0264	-2.7867	1304	7	1917899	1.76
BLG105	$18^{h}01^{m}39.^{s}6$	$-29^\circ28'12''$	1.3138	-3.2882	928	16	1950115	1.73
BLG106	$17^{h}46^{m}29.^{s}6$	$-37^\circ09'46''$	353.0553	-4.4247	130	3	1160605	1.58
BLG107	$17^{h}49^{m}22.^{s}6$	$-37^\circ09'45''$	353.3508	-4.9179	128	2	1100541	1.47
BLG108	$17^{h}46^{m}29.^{s}3$	$-36^\circ34'09''$	353.5649	-4.1178	307	3	1330549	1.72
BLG109	$17^{h}49^{m}21.^{s}4$	$-36^\circ34'11''$	353.8606	-4.6125	142	3	1156136	1.53
BLG110	$17^{h}52^{m}13.^{s}4$	$-36^\circ34'11''$	354.1533	-5.1087	127	3	1306752	1.43
BLG111	$17^{h}55^{m}05.^{s}4$	$-36^\circ34'11''$	354.4427	-5.6070	124	3	1090425	1.43
BLG112	$17^{h}46^{m}30.^{s}1$	$-35^\circ59'04''$	354.0683	-3.8184	266	3	1158383	1.78
BLG113	$17^{h}49^{m}19.^{s}8$	$-35^\circ59'04''$	354.3628	-4.3094	246	3	1281475	1.49
BLG114	$17^{h}52^{m}10.^{s}0$	$-35^\circ59'04''$	354.6549	-4.8038	207	3	1155206	1.35
BLG115	$17^{h}54^{m}59.^{s}1$	$-35^\circ58'46''$	354.9463	-5.2946	230	3	1204776	1.41
BLG116	$17^{h}46^{m}28.^{s}9$	$-35^\circ23'15''$	354.5784	-3.5065	208	2	1188410	1.67
BLG117	$17^{h}49^{m}17.^{s}7$	$-35^\circ23'16''$	354.8735	-3.9985	315	2	1270330	1.52
BLG118	$17^{h}52^{m}06.^{s}8$	$-35^\circ23'17''$	355.1659	-4.4934	209	3	1335721	1.38
BLG119	$17^{h}54^{m}55.^{s}7$	$-35^\circ23'17''$	355.4551	-4.9895	250	3	1232697	1.44
BLG120	$17^{h}57^{m}44.^{s}7$	$-35^\circ23'17''$	355.7413	-5.4878	126	3	1245666	1.40
BLG121	$17^{h}46^{m}28.^{s}2$	$-34^\circ47'43''$	355.0849	-3.1982	650	5	1736742	1.77
BLG122	$17^{h}49^{m}17.^{s}3$	$-34^\circ47'50''$	355.3814	-3.6954	942	23	1722815	1.60
BLG123	$17^{h}52^{m}05.^{s}1$	$-34^\circ47'52''$	355.6737	-4.1900	123	3	1588137	1.41
BLG124	$17^{h}54^{m}53.^{s}3$	$-34^\circ47'52''$	355.9641	-4.6874	122	2	1429450	1.47
BLG125	$17^{h}57^{m}40.^{s}1$	$-34^\circ47'45''$	356.2507	-5.1815	123	2	1408780	1.32
BLG126	$18^{h}00^{m}28.^{s}4$	$-34^\circ47'45''$	356.5351	-5.6830	121	2	1289096	1.27
BLG127	$18^{h}03^{m}16.^{s}0$	$-34^\circ47'45''$	356.8153	-6.1841	118	2	1073591	1.20
BLG128	$18^{h}06^{m}03.^{s}9$	$-34^\circ47'45''$	357.0931	-6.6880	116	2	1020448	1.16
BLG129	$17^{h}43^{m}43.^{s}2$	$-34^\circ12'11''$	355.2961	-2.4063	873	4	1518947	2.09
BLG130	$17^{h}46^{m}30.^{s}3$	$-34^\circ12'12''$	355.5959	-2.8981	816	5	1580442	1.97
BLG131	$17^{h}49^{m}17.^{s}3$	$-34^\circ12'12''$	355.8926	-3.3915	645	5	1502103	1.87
BLG132	$17^{h}52^{m}04.^{s}3$	$-34^\circ12'14''$	356.1858	-3.8870	319	3	1693143	1.71
BLG133	$17^{h}54^{m}51.^{s}3$	$-34^\circ12'14''$	356.4764	-4.3842	327	3	1714126	1.48
BLG134	$17^{h}57^{m}38.^{s}2$	$-34^\circ12'14''$	356.7638	-4.8829	326	3	1702292	1.35
BLG135	$18^{h}00^{m}25.^{s}2$	$-34^\circ12'14''$	357.0484	-5.3838	118	2	1335327	1.39
BLG136	$18^{h}03^{m}12.^{s}0$	$-34^\circ12'14''$	357.3296	-5.8858	114	2	1176068	1.35
BLG137	$18^{h}05^{m}59.^{s}0$	$-34^\circ12'14''$	357.6083	-6.3902	112	2	1089365	1.21
BLG138	$17^{h}45^{m}14.^{s}8$	$-33^\circ36'41''$	355.9667	-2.3677	903	8	1410387	2.27
BLG139	$17^{h}47^{m}59.^{s}7$	$-33^\circ36'42''$	356.2631	-2.8574	803	6	1411746	2.17
BLG140	$17^{h}50^{m}44.^{s}7$	$-33^\circ36'52''$	356.5544	-3.3505	629	6	1349063	2.13
BLG141	$17^{h}53^{m}29.^{s}9$	$-33^\circ36'47''$	356.8467	-3.8439	619	5	1503940	1.89
BLG142	$17^{h}56^{m}15.^{s}2$	$-33^\circ37'03''$	357.1312	-4.3424	685	6	1597926	1.60
BLG143	$17^{h}59^{m}00.^{s}2$	$-33^\circ37'03''$	357.4160	-4.8396	118	2	1366023	1.56

T a b l e 1

Continued

Field	RA	Dec (J2000)	l_{II}	b_{II}	Nfr$_I$	Nfr$_V$	Nobj	$\langle V-I \rangle$
BLG144	$18^{h}01^{m}44.^{s}6$	$-33^\circ36'46''$	357.7011	-5.3344	119	2	1261419	1.50
BLG145	$18^{h}04^{m}29.^{s}6$	$-33^\circ36'45''$	357.9805	-5.8349	118	2	1176674	1.33
BLG146	$18^{h}07^{m}14.^{s}5$	$-33^\circ36'46''$	358.2563	-6.3371	116	2	1056951	1.23
BLG147	$17^{h}49^{m}45.^{s}0$	$-33^\circ01'31''$	356.9554	-2.8709	798	5	1608385	2.27
BLG148	$17^{h}52^{m}36.^{s}3$	$-33^\circ01'32''$	357.2603	-3.3861	797	14	1660863	1.98
BLG149	$17^{h}55^{m}15.^{s}2$	$-33^\circ01'33''$	357.5402	-3.8657	669	19	1301727	1.84
BLG150	$17^{h}58^{m}00.^{s}3$	$-33^\circ01'33''$	357.8285	-4.3657	316	6	1485986	1.75
BLG151	$18^{h}00^{m}45.^{s}3$	$-33^\circ01'31''$	358.1142	-4.8669	116	2	1381823	1.66
BLG152	$18^{h}03^{m}28.^{s}9$	$-33^\circ01'14''$	358.3982	-5.3635	114	2	1322100	1.51
BLG153	$18^{h}06^{m}15.^{s}4$	$-33^\circ01'31''$	358.6761	-5.8753	112	2	1202493	1.38
BLG154	$18^{h}09^{m}00.^{s}4$	$-33^\circ01'31''$	358.9527	-6.3818	115	2	1040092	1.28
BLG155	$17^{h}52^{m}17.^{s}6$	$-32^\circ25'59''$	357.7386	-3.0292	833	5	1776618	2.16
BLG156	$17^{h}55^{m}00.^{s}6$	$-32^\circ26'00''$	358.0281	-3.5242	829	5	1831359	1.96
BLG157	$17^{h}57^{m}43.^{s}8$	$-32^\circ26'00''$	358.3155	-4.0214	940	17	1596728	1.81
BLG158	$18^{h}00^{m}26.^{s}7$	$-32^\circ26'02''$	358.5989	-4.5197	338	3	1468191	1.68
BLG159	$18^{h}03^{m}09.^{s}8$	$-32^\circ26'01''$	358.8807	-5.0198	116	2	1277414	1.55
BLG160	$18^{h}05^{m}52.^{s}9$	$-32^\circ26'01''$	359.1595	-5.5218	208	2	1144288	1.51
BLG161	$18^{h}08^{m}35.^{s}8$	$-32^\circ26'00''$	359.4354	-6.0246	114	3	1018260	1.41
BLG162	$18^{h}11^{m}18.^{s}7$	$-32^\circ26'00''$	359.7083	-6.5291	113	2	1007827	1.35
BLG163	$17^{h}52^{m}44.^{s}6$	$-31^\circ50'13''$	358.3014	-2.8090	774	4	1471605	2.33
BLG164	$17^{h}55^{m}26.^{s}6$	$-31^\circ50'12''$	358.5912	-3.3041	766	4	1752969	1.94
BLG165	$17^{h}58^{m}08.^{s}5$	$-31^\circ50'13''$	358.8776	-3.8008	382	6	1693738	2.04
BLG166	$18^{h}00^{m}50.^{s}6$	$-31^\circ50'14''$	359.1616	-4.2998	326	4	1785605	1.67
BLG167	$18^{h}03^{m}32.^{s}6$	$-31^\circ50'15''$	359.4427	-4.8001	360	2	1502055	1.56
BLG168	$18^{h}06^{m}14.^{s}6$	$-31^\circ50'17''$	359.7208	-5.3022	112	2	1393456	1.41
BLG169	$18^{h}08^{m}56.^{s}5$	$-31^\circ50'19''$	359.9961	-5.8055	113	3	1106519	1.40
BLG170	$18^{h}11^{m}38.^{s}5$	$-31^\circ50'18''$	0.2696	-6.3104	110	3	1129678	1.30
BLG171	$17^{h}52^{m}44.^{s}1$	$-31^\circ14'47''$	358.8100	-2.5080	927	5	1562062	2.42
BLG172	$17^{h}55^{m}25.^{s}0$	$-31^\circ14'47''$	359.0997	-3.0028	1406	6	1797708	1.97
BLG173	$17^{h}58^{m}06.^{s}0$	$-31^\circ14'48''$	359.3865	-3.4997	786	5	1580697	2.03
BLG174	$18^{h}00^{m}46.^{s}9$	$-31^\circ14'48''$	359.6707	-3.9978	344	2	1651630	1.85
BLG175	$18^{h}03^{m}27.^{s}8$	$-31^\circ14'48''$	359.9522	-4.4975	384	3	1477697	1.72
BLG176	$18^{h}06^{m}08.^{s}9$	$-31^\circ14'48''$	0.2313	-4.9995	355	2	1405589	1.56
BLG177	$18^{h}08^{m}49.^{s}7$	$-31^\circ14'49''$	0.5071	-5.5022	115	3	1326372	1.39
BLG178	$18^{h}11^{m}32.^{s}2$	$-31^\circ14'55''$	0.7819	-6.0124	114	3	1192805	1.33
BLG179	$17^{h}50^{m}00.^{s}0$	$-30^\circ39'17''$	359.0200	-1.7019	1428	3	1110253	2.86
BLG180	$17^{h}52^{m}39.^{s}8$	$-30^\circ39'20''$	359.3117	-2.1949	1463	9	1761449	2.41
BLG181	$17^{h}55^{m}19.^{s}7$	$-30^\circ39'18''$	359.6020	-2.6892	1303	5	1727735	2.11
BLG182	$17^{h}58^{m}00.^{s}1$	$-30^\circ39'17''$	359.8903	-3.1869	1433	8	1501630	2.12
BLG183	$18^{h}00^{m}39.^{s}6$	$-30^\circ39'17''$	0.1741	-3.6835	803	5	1664547	1.82
BLG184	$18^{h}03^{m}18.^{s}0$	$-30^\circ39'19''$	0.4528	-4.1785	768	5	1611072	1.77
BLG185	$18^{h}06^{m}00.^{s}6$	$-30^\circ39'19''$	0.7367	-4.6880	821	4	1685043	1.64
BLG186	$18^{h}08^{m}39.^{s}7$	$-30^\circ39'16''$	1.0127	-5.1876	111	4	1377094	1.45
BLG187	$18^{h}11^{m}19.^{s}8$	$-30^\circ39'14''$	1.2876	-5.6920	107	2	1281754	1.27
BLG188	$17^{h}59^{m}00.^{s}2$	$-30^\circ03'59''$	0.5091	-3.0819	814	8	1917577	1.81

Table 1

Continued

Field	RA	Dec (J2000)	l_{II}	b_{II}	Nfr$_I$	Nfr$_V$	Nobj	$\langle V-I\rangle$
BLG189	$18^{\mathrm{h}}01^{\mathrm{m}}39.^{\mathrm{s}}1$	$-30^\circ03'57''$	0.7932	−3.5798	776	12	1890245	1.59
BLG190	$18^{\mathrm{h}}04^{\mathrm{m}}28.^{\mathrm{s}}1$	$-30^\circ03'56''$	1.0922	−4.1112	1003	15	1685701	1.48
BLG191	$18^{\mathrm{h}}07^{\mathrm{m}}07.^{\mathrm{s}}0$	$-30^\circ03'56''$	1.3705	−4.6125	110	3	1537932	1.51
BLG192	$18^{\mathrm{h}}09^{\mathrm{m}}45.^{\mathrm{s}}9$	$-30^\circ03'56''$	1.6463	−5.1153	108	2	1416159	1.42
BLG193	$18^{\mathrm{h}}12^{\mathrm{m}}25.^{\mathrm{s}}0$	$-30^\circ03'57''$	1.9196	−5.6204	194	2	1368305	1.28
BLG194	$17^{\mathrm{h}}50^{\mathrm{m}}59.^{\mathrm{s}}8$	$-29^\circ24'27''$	0.2022	−1.2486	1379	11	1114100	2.62
BLG195	$17^{\mathrm{h}}53^{\mathrm{m}}38.^{\mathrm{s}}4$	$-29^\circ14'20''$	0.6407	−1.6588	1354	8	1937546	2.33
BLG196	$18^{\mathrm{h}}04^{\mathrm{m}}27.^{\mathrm{s}}3$	$-29^\circ28'06''$	1.6137	−3.8178	1298	14	1833526	1.54
BLG197	$18^{\mathrm{h}}07^{\mathrm{m}}04.^{\mathrm{s}}3$	$-29^\circ28'22''$	1.8867	−4.3181	915	6	1659192	1.52
BLG198	$18^{\mathrm{h}}09^{\mathrm{m}}42.^{\mathrm{s}}3$	$-29^\circ28'22''$	2.1628	−4.8208	766	5	1573823	1.40
BLG199	$18^{\mathrm{h}}12^{\mathrm{m}}20.^{\mathrm{s}}3$	$-29^\circ28'22''$	2.4365	−5.3250	114	3	1530714	1.28
BLG200	$17^{\mathrm{h}}26^{\mathrm{m}}59.^{\mathrm{s}}7$	$-39^\circ54'52''$	348.6826	−2.6778	117	2	887388	1.88
BLG201	$17^{\mathrm{h}}27^{\mathrm{m}}00.^{\mathrm{s}}1$	$-39^\circ19'30''$	349.1736	−2.3510	114	2	908803	2.13
BLG202	$17^{\mathrm{h}}29^{\mathrm{m}}58.^{\mathrm{s}}6$	$-39^\circ54'58''$	348.9976	−3.1552	111	2	831860	1.89
BLG203	$17^{\mathrm{h}}29^{\mathrm{m}}59.^{\mathrm{s}}1$	$-39^\circ19'30''$	349.4930	−2.8317	111	3	854256	2.05
BLG204	$18^{\mathrm{h}}14^{\mathrm{m}}59.^{\mathrm{s}}9$	$-29^\circ28'21''$	2.7107	−5.8355	110	3	1397880	1.18
BLG205	$17^{\mathrm{h}}57^{\mathrm{m}}16.^{\mathrm{s}}4$	$-28^\circ53'10''$	1.3456	−2.1672	1394	34	2275476	2.05
BLG206	$17^{\mathrm{h}}59^{\mathrm{m}}52.^{\mathrm{s}}8$	$-28^\circ53'00''$	1.6324	−2.6606	1363	18	2183459	1.62
BLG207	$18^{\mathrm{h}}02^{\mathrm{m}}33.^{\mathrm{s}}4$	$-28^\circ52'58''$	1.9223	−3.1700	1120	19	2002261	1.57
BLG208	$18^{\mathrm{h}}05^{\mathrm{m}}08.^{\mathrm{s}}4$	$-28^\circ53'00''$	2.1987	−3.6636	1399	41	1894677	1.52
BLG209	$18^{\mathrm{h}}07^{\mathrm{m}}43.^{\mathrm{s}}9$	$-28^\circ53'00''$	2.4741	−4.1600	108	4	1748973	1.50
BLG210	$18^{\mathrm{h}}10^{\mathrm{m}}22.^{\mathrm{s}}1$	$-28^\circ53'00''$	2.7518	−4.6664	23	2	1409499	1.43
BLG211	$18^{\mathrm{h}}12^{\mathrm{m}}59.^{\mathrm{s}}1$	$-28^\circ53'00''$	3.0250	−5.1704	22	2	1237744	1.30
BLG212	$18^{\mathrm{h}}15^{\mathrm{m}}36.^{\mathrm{s}}6$	$-28^\circ52'58''$	3.2972	−5.6771	102	3	1420104	1.25
BLG213	$18^{\mathrm{h}}18^{\mathrm{m}}13.^{\mathrm{s}}1$	$-28^\circ53'00''$	3.5644	−6.1825	20	4	1073979	1.25
BLG214	$17^{\mathrm{h}}57^{\mathrm{m}}32.^{\mathrm{s}}6$	$-28^\circ17'25''$	1.8915	−1.9205	1206	8	1862536	2.28
BLG215	$18^{\mathrm{h}}00^{\mathrm{m}}09.^{\mathrm{s}}7$	$-28^\circ17'26''$	2.1784	−2.4206	1082	8	1974275	1.86
BLG216	$18^{\mathrm{h}}02^{\mathrm{m}}44.^{\mathrm{s}}5$	$-28^\circ17'29''$	2.4582	−2.9150	1044	6	2010062	1.63
BLG217	$18^{\mathrm{h}}05^{\mathrm{m}}19.^{\mathrm{s}}6$	$-28^\circ17'27''$	2.7373	−3.4111	821	10	1921363	1.56
BLG218	$18^{\mathrm{h}}07^{\mathrm{m}}55.^{\mathrm{s}}4$	$-28^\circ17'28''$	3.0146	−3.9113	678	5	1713709	1.65
BLG219	$18^{\mathrm{h}}10^{\mathrm{m}}30.^{\mathrm{s}}1$	$-28^\circ17'32''$	3.2868	−4.4098	777	5	1647078	1.48
BLG220	$18^{\mathrm{h}}13^{\mathrm{m}}06.^{\mathrm{s}}0$	$-28^\circ17'32''$	3.5598	−4.9129	200	3	1717223	1.27
BLG221	$18^{\mathrm{h}}15^{\mathrm{m}}42.^{\mathrm{s}}1$	$-28^\circ17'32''$	3.8308	−5.4180	115	3	1557697	1.20
BLG222	$18^{\mathrm{h}}18^{\mathrm{m}}18.^{\mathrm{s}}0$	$-28^\circ17'30''$	4.0997	−5.9236	116	4	1347613	1.23
BLG223	$17^{\mathrm{h}}59^{\mathrm{m}}19.^{\mathrm{s}}7$	$-27^\circ41'56''$	2.6011	−1.9671	1323	30	1692197	2.28
BLG224	$18^{\mathrm{h}}01^{\mathrm{m}}55.^{\mathrm{s}}2$	$-27^\circ41'56''$	2.8853	−2.4656	1033	6	1916029	1.90
BLG225	$18^{\mathrm{h}}04^{\mathrm{m}}30.^{\mathrm{s}}2$	$-27^\circ41'58''$	3.1657	−2.9641	825	6	2159774	1.65
BLG226	$18^{\mathrm{h}}07^{\mathrm{m}}05.^{\mathrm{s}}4$	$-27^\circ41'59''$	3.4443	−3.4645	847	6	2078177	1.51
BLG227	$18^{\mathrm{h}}09^{\mathrm{m}}39.^{\mathrm{s}}6$	$-27^\circ41'59''$	3.7191	−3.9629	787	4	1986367	1.49
BLG228	$18^{\mathrm{h}}12^{\mathrm{m}}15.^{\mathrm{s}}1$	$-27^\circ42'00''$	3.9937	−4.4670	18	3	1314414	1.33
BLG229	$18^{\mathrm{h}}14^{\mathrm{m}}50.^{\mathrm{s}}1$	$-27^\circ42'00''$	4.2653	−4.9707	18	3	1159502	1.20
BLG230	$18^{\mathrm{h}}17^{\mathrm{m}}25.^{\mathrm{s}}1$	$-27^\circ42'00''$	4.5347	−5.4757	17	2	1179505	1.26
BLG231	$18^{\mathrm{h}}20^{\mathrm{m}}00.^{\mathrm{s}}1$	$-27^\circ42'00''$	4.8019	−5.9820	17	5	1052213	1.32
BLG232	$17^{\mathrm{h}}59^{\mathrm{m}}59.^{\mathrm{s}}7$	$-27^\circ06'25''$	3.1886	−1.8015	745	4	1557796	2.42
BLG233	$18^{\mathrm{h}}02^{\mathrm{m}}37.^{\mathrm{s}}0$	$-27^\circ06'24''$	3.4774	−2.3085	623	3	1739011	2.31

Table 1

Continued

Field	RA	Dec (J2000)	l_{II}	b_{II}	Nfr$_I$	Nfr$_V$	Nobj	$\langle V-I\rangle$
BLG234	$18^h05^m12\overset{s}{.}1$	$-27°06'25''$	3.7592	−2.8102	640	5	1981513	1.66
BLG235	$18^h07^m47\overset{s}{.}1$	$-27°06'26''$	4.0386	−3.3128	685	20	1823097	1.65
BLG236	$18^h10^m20\overset{s}{.}1$	$-27°06'28''$	4.3118	−3.8105	300	2	1772717	1.71
BLG237	$18^h12^m55\overset{s}{.}2$	$-27°06'29''$	4.5867	−4.3162	105	7	1642632	1.40
BLG238	$18^h15^m29\overset{s}{.}7$	$-27°06'29''$	4.8586	−4.8211	106	6	1553326	1.33
BLG239	$18^h18^m05\overset{s}{.}1$	$-27°06'30''$	5.1296	−5.3303	15	2	1093822	1.35
BLG240	$18^h20^m39\overset{s}{.}8$	$-27°06'30''$	5.3975	−5.8384	14	2	975542	1.39
BLG241	$18^h06^m02\overset{s}{.}2$	$-26°30'52''$	4.3681	−2.6842	790	13	1633314	1.97
BLG242	$18^h08^m36\overset{s}{.}3$	$-26°30'53''$	4.6467	−3.1869	564	5	1882684	1.84
BLG243	$18^h11^m10\overset{s}{.}3$	$-26°30'55''$	4.9226	−3.6907	187	3	1503175	1.66
BLG244	$18^h13^m44\overset{s}{.}4$	$-26°30'56''$	5.1967	−4.1959	171	4	1440633	1.52
BLG245	$18^h16^m18\overset{s}{.}5$	$-26°30'56''$	5.4689	−4.7024	15	3	1126469	1.44
BLG246	$18^h18^m49\overset{s}{.}0$	$-26°30'59''$	5.7319	−5.1986	104	3	1350870	1.42
BLG247	$18^h21^m24\overset{s}{.}1$	$-26°31'00''$	6.0014	−5.7109	14	2	853708	1.46
BLG248	$18^h23^m58\overset{s}{.}1$	$-26°30'59''$	6.2673	−6.2205	103	2	1092107	1.28
BLG249	$18^h06^m00\overset{s}{.}2$	$-25°55'18''$	4.8827	−2.3890	588	5	1477672	2.30
BLG250	$18^h08^m32\overset{s}{.}6$	$-25°55'26''$	5.1581	−2.8895	509	4	1723868	1.92
BLG251	$18^h11^m07\overset{s}{.}5$	$-25°55'27''$	5.4376	−3.3985	551	4	1553925	1.72
BLG252	$18^h13^m39\overset{s}{.}1$	$-25°55'20''$	5.7108	−3.8968	259	2	1405414	1.67
BLG253	$18^h16^m11\overset{s}{.}9$	$-25°55'21''$	5.9822	−4.4015	108	2	1459393	1.45
BLG254	$18^h18^m45\overset{s}{.}0$	$-25°55'21''$	6.2522	−4.9082	108	9	1342950	1.42
BLG255	$18^h21^m18\overset{s}{.}7$	$-25°55'30''$	6.5190	−5.4192	108	2	1158691	1.49
BLG256	$18^h23^m51\overset{s}{.}6$	$-25°55'31''$	6.7843	−5.9277	103	2	1101295	1.41
BLG257	$18^h08^m30\overset{s}{.}0$	$-25°19'48''$	5.6739	−2.5939	109	2	1485247	2.12
BLG258	$18^h11^m01\overset{s}{.}8$	$-25°19'49''$	5.9493	−3.0950	107	2	1487206	2.03
BLG259	$18^h13^m33\overset{s}{.}8$	$-25°19'49''$	6.2232	−3.5979	105	2	1331882	1.92
BLG260	$18^h16^m06\overset{s}{.}1$	$-25°20'00''$	6.4929	−4.1045	99	3	1499790	1.64
BLG261	$18^h18^m38\overset{s}{.}1$	$-25°20'00''$	6.7627	−4.6098	100	2	1368037	1.44
BLG262	$18^h21^m09\overset{s}{.}9$	$-25°19'59''$	7.0303	−5.1154	97	2	1218733	1.38
BLG263	$18^h23^m41\overset{s}{.}7$	$-25°20'00''$	7.2955	−5.6225	99	5	1171702	1.41
BLG264	$18^h26^m13\overset{s}{.}7$	$-25°20'00''$	7.5593	−6.1312	98	3	915042	1.40
BLG265	$18^h14^m29\overset{s}{.}4$	$-24°44'27''$	6.8428	−3.5025	106	4	1329570	1.86
BLG266	$18^h17^m01\overset{s}{.}4$	$-24°44'27''$	7.1154	−4.0093	102	5	1324518	1.72
BLG267	$18^h19^m34\overset{s}{.}1$	$-24°44'30''$	7.3865	−4.5200	21	4	886425	1.53
BLG268	$18^h22^m06\overset{s}{.}1$	$-24°44'30''$	7.6551	−5.0291	22	4	878867	1.46
BLG269	$18^h24^m38\overset{s}{.}1$	$-24°44'30''$	7.9217	−5.5394	23	4	973815	1.41
BLG270	$18^h27^m10\overset{s}{.}1$	$-24°44'30''$	8.1864	−6.0507	22	13	877532	1.43
BLG271	$18^h29^m42\overset{s}{.}1$	$-24°44'30''$	8.4493	−6.5632	20	3	675396	1.37
BLG272	$18^h16^m00\overset{s}{.}1$	$-24°09'00''$	7.5274	−3.5254	21	3	1039961	1.87
BLG273	$18^h18^m31\overset{s}{.}1$	$-24°09'00''$	7.7985	−4.0318	21	5	1096212	1.55
BLG274	$18^h21^m02\overset{s}{.}1$	$-24°09'00''$	8.0677	−4.5393	20	3	990320	1.49
BLG275	$18^h23^m33\overset{s}{.}1$	$-24°09'00''$	8.3349	−5.0479	20	5	847642	1.53
BLG276	$18^h26^m04\overset{s}{.}1$	$-24°09'00''$	8.6003	−5.5575	23	4	762870	1.52
BLG277	$18^h28^m35\overset{s}{.}1$	$-24°09'00''$	8.8638	−6.0683	22	5	733393	1.54
BLG278	$18^h31^m04\overset{s}{.}9$	$-24°08'58''$	9.1240	−6.5758	100	2	756314	1.49

Table 1

Continued

Field	RA	Dec (J2000)	l_{II}	b_{II}	Nfr$_I$	Nfr$_V$	Nobj	$\langle V-I\rangle$
BLG279	$18^h16^m00\overset{s}{.}1$	$-23°33'30''$	8.0495	−3.2454	20	4	1011305	1.81
BLG280	$18^h18^m30\overset{s}{.}1$	$-23°33'30''$	8.3203	−3.7505	19	4	989315	1.68
BLG281	$18^h21^m00\overset{s}{.}1$	$-23°33'30''$	8.5891	−4.2568	19	3	949372	1.54
BLG282	$18^h23^m30\overset{s}{.}1$	$-23°33'30''$	8.8561	−4.7641	17	3	800872	1.60
BLG283	$18^h26^m00\overset{s}{.}1$	$-23°33'30''$	9.1213	−5.2725	18	5	749195	1.51
BLG284	$18^h28^m30\overset{s}{.}1$	$-23°33'30''$	9.3847	−5.7819	18	3	657775	1.52
BLG285	$18^h31^m00\overset{s}{.}1$	$-23°33'30''$	9.6463	−6.2923	18	3	603916	1.47
BLG286	$18^h16^m00\overset{s}{.}1$	$-22°58'00''$	8.5713	−2.9651	17	4	915277	1.99
BLG287	$18^h18^m30\overset{s}{.}1$	$-22°58'00''$	8.8435	−3.4723	16	4	911160	1.81
BLG288	$18^h21^m00\overset{s}{.}1$	$-22°58'00''$	9.1138	−3.9807	16	4	881015	1.66
BLG289	$18^h23^m30\overset{s}{.}1$	$-22°58'00''$	9.3822	−4.4901	18	4	898691	1.57
BLG290	$18^h26^m00\overset{s}{.}1$	$-22°58'00''$	9.6489	−5.0005	14	3	788157	1.54
BLG291	$18^h28^m30\overset{s}{.}1$	$-22°58'00''$	9.9138	−5.5120	14	5	672798	1.49
BLG292	$18^h31^m00\overset{s}{.}1$	$-22°58'00''$	10.1769	−6.0244	15	5	614425	1.43
BLG293	$18^h16^m00\overset{s}{.}1$	$-22°22'30''$	9.0929	−2.6845	16	11	1040978	2.19
BLG294	$18^h18^m29\overset{s}{.}1$	$-22°22'30''$	9.3646	−3.1905	16	3	1021042	1.91
BLG295	$18^h20^m58\overset{s}{.}1$	$-22°22'30''$	9.6345	−3.6974	17	3	951091	1.78
BLG296	$18^h23^m27\overset{s}{.}1$	$-22°22'30''$	9.9026	−4.2054	15	5	936343	1.64
BLG297	$18^h25^m56\overset{s}{.}1$	$-22°22'30''$	10.1689	−4.7144	15	4	869260	1.45
BLG298	$18^h28^m25\overset{s}{.}1$	$-22°22'30''$	10.4335	−5.2244	13	3	838656	1.30
BLG299	$18^h30^m54\overset{s}{.}1$	$-22°22'30''$	10.6964	−5.7354	14	3	726365	1.34
BLG300	$18^h17^m00\overset{s}{.}1$	$-21°47'00''$	9.7244	−2.6082	17	3	1007743	2.00
BLG301	$18^h19^m28\overset{s}{.}1$	$-21°47'00''$	9.9948	−3.1131	17	3	892601	1.96
BLG302	$18^h21^m56\overset{s}{.}1$	$-21°47'00''$	10.2635	−3.6190	18	4	882631	1.95
BLG303	$18^h24^m24\overset{s}{.}1$	$-21°47'00''$	10.5305	−4.1260	17	5	934256	1.63
BLG304	$18^h26^m52\overset{s}{.}1$	$-21°47'00''$	10.7957	−4.6339	15	6	763531	1.56
BLG305	$18^h29^m19\overset{s}{.}8$	$-21°47'00''$	11.0588	−5.1417	16	5	694849	1.39
BLG306	$18^h31^m48\overset{s}{.}1$	$-21°47'00''$	11.3213	−5.6525	16	6	720132	1.42
BLG307	$18^h23^m10\overset{s}{.}1$	$-21°11'30''$	10.9220	−3.5970	18	3	780694	1.86
BLG308	$18^h25^m38\overset{s}{.}1$	$-21°11'30''$	11.1894	−4.1063	16	3	666080	1.75
BLG309	$18^h28^m06\overset{s}{.}1$	$-21°11'30''$	11.4552	−4.6166	16	4	655837	1.63
BLG310	$18^h30^m34\overset{s}{.}1$	$-21°11'30''$	11.7194	−5.1278	17	4	626459	1.64
BLG311	$18^h33^m02\overset{s}{.}1$	$-21°11'30''$	11.9820	−5.6399	17	4	568079	1.46
BLG312	$18^h24^m39\overset{s}{.}8$	$-20°36'00''$	11.6095	−3.6311	20	4	814800	1.89
BLG313	$18^h27^m07\overset{s}{.}1$	$-20°36'00''$	11.8760	−4.1404	19	4	682459	1.86
BLG314	$18^h33^m00\overset{s}{.}1$	$-20°36'00''$	12.5082	−5.3646	19	4	608451	1.49
BLG315	$17^h52^m16\overset{s}{.}1$	$-37°10'00''$	353.6398	−5.4169	19	2	797278	1.46
BLG316	$17^h45^m00\overset{s}{.}1$	$-37°45'30''$	352.3905	−4.4789	19	2	710766	1.80
BLG317	$17^h47^m54\overset{s}{.}1$	$-37°45'30''$	352.6865	−4.9703	18	2	734776	1.56
BLG318	$17^h50^m47\overset{s}{.}9$	$-37°45'21''$	352.9810	−5.4620	123	2	955689	1.47
BLG319	$17^h47^m30\overset{s}{.}1$	$-38°21'00''$	352.1357	−5.2054	19	2	756243	1.51
BLG320	$17^h50^m26\overset{s}{.}1$	$-38°21'00''$	352.4295	−5.7005	19	3	769101	1.40
BLG321	$17^h53^m22\overset{s}{.}1$	$-38°21'00''$	352.7199	−6.1979	20	3	636272	1.38
BLG322	$17^h46^m00\overset{s}{.}1$	$-38°56'30''$	351.4748	−5.2575	20	4	734816	1.54
BLG323	$17^h48^m57\overset{s}{.}1$	$-38°56'30''$	351.7694	−5.7506	20	3	706144	1.35

Table 1

Concluded

Field	RA	Dec (J2000)	l_{II}	b_{II}	Nfr_I	Nfr_V	Nobj	$\langle V-I\rangle$
BLG324	$17^h51^m54.^s1$	$-38°56'30''$	352.0604	−6.2458	19	3	603439	1.36
BLG325	$17^h38^m30.^s1$	$-39°32'00''$	350.2073	−4.3283	22	3	570310	1.65
BLG326	$17^h41^m29.^s1$	$-39°32'00''$	350.5114	−4.8171	20	4	570484	1.62
BLG327	$17^h44^m28.^s1$	$-39°32'00''$	350.8120	−5.3083	20	3	566849	1.51
BLG328	$17^h47^m27.^s1$	$-39°32'00''$	351.1089	−5.8018	20	3	556223	1.36
BLG329	$17^h50^m26.^s1$	$-39°32'00''$	351.4022	−6.2976	19	2	540815	1.32
BLG330	$17^h28^m00.^s1$	$-29°30'00''$	357.4584	2.9392	113	3	1489220	2.31
BLG331	$17^h24^m50.^s1$	$-29°20'00''$	357.2127	3.6048	110	15	1514420	2.12
BLG332	$17^h10^m00.^s5$	$-32°59'50''$	352.3810	4.0909	111	5	1015348	1.64
BLG333	$17^h35^m30.^s1$	$-27°10'01''$	0.3176	2.8305	359	6	1270794	2.61
BLG334	$17^h41^m40.^s2$	$-24°59'53''$	2.8940	2.8132	107	7	1338590	2.57
BLG335	$17^h34^m32.^s9$	$-22°29'56''$	4.1485	5.5217	115	7	1007985	1.84
BLG336	$17^h37^m02.^s0$	$-22°29'58''$	4.4558	5.0361	114	6	1040076	1.97
BLG337	$17^h39^m31.^s0$	$-22°29'58''$	4.7608	4.5497	116	13	1087002	2.04
BLG338	$17^h42^m00.^s0$	$-22°29'59''$	5.0632	4.0618	113	6	1219047	1.98
BLG339	$17^h47^m00.^s0$	$-22°29'59''$	5.6653	3.0756	412	3	1261835	1.98
BLG340	$17^h49^m30.^s2$	$-22°29'54''$	5.9644	2.5806	314	3	1185439	2.25
BLG341	$17^h51^m57.^s9$	$-22°29'59''$	6.2539	2.0911	109	5	1260449	2.38
BLG342	$17^h46^m29.^s7$	$-23°05'22''$	5.0996	2.8703	325	3	1372416	1.92
BLG343	$17^h48^m59.^s8$	$-23°05'21''$	5.3969	2.3775	318	3	1295253	2.15
BLG344	$17^h43^m30.^s3$	$-23°40'55''$	4.2355	3.1480	251	3	1503135	2.04
BLG345	$17^h46^m00.^s4$	$-23°40'56''$	4.5339	2.6589	109	2	1458394	2.06
BLG346	$17^h42^m00.^s3$	$-24°16'29''$	3.5501	3.1290	332	3	1457492	2.15
BLG347	$17^h44^m31.^s3$	$-24°16'25''$	3.8517	2.6410	314	3	1400744	2.23
BLG348	$17^h44^m30.^s2$	$-20°04'55''$	7.4377	4.8242	114	2	1001745	1.68
BLG349	$17^h45^m31.^s2$	$-19°29'30''$	8.0689	4.9247	108	2	896882	1.71
BLG350	$17^h47^m50.^s2$	$-21°00'00''$	7.0531	3.6820	109	2	1138004	1.91
BLG351	$17^h43^m20.^s2$	$-21°29'50''$	6.0825	4.3217	103	2	1166359	1.80
BLG352	$17^h39^m20.^s2$	$-21°04'56''$	5.9472	5.3327	183	2	1055393	1.64
BLG353	$17^h49^m30.^s2$	$-17°39'59''$	10.1278	5.0490	101	6	767562	1.59
BLG354	$17^h35^m01.^s4$	$-23°34'58''$	3.2886	4.8483	307	3	1132575	2.09
BLG355	$17^h26^m00.^s2$	$-25°24'56''$	0.6228	5.5703	107	10	1040564	1.86
BLG356	$17^h25^m00.^s1$	$-27°44'51''$	358.5517	4.4605	106	6	1181464	2.09
BLG357	$17^h23^m50.^s3$	$-25°59'52''$	359.8641	5.6521	105	3	1067907	1.69
BLG358	$17^h18^m59.^s8$	$-29°00'05''$	356.7655	4.8440	133	7	1297380	1.74
BLG359	$17^h16^m23.^s1$	$-29°00'00''$	356.4383	5.3130	21	5	1026221	1.65
BLG360	$17^h13^m45.^s5$	$-29°00'06''$	356.1036	5.7808	111	17	1010778	1.55
BLG361	$17^h19^m00.^s1$	$-29°35'30''$	356.2797	4.5064	19	7	988799	1.95
BLG362	$17^h16^m22.^s1$	$-29°35'30''$	355.9504	4.9754	20	6	1046220	1.79
BLG363	$17^h13^m43.^s5$	$-29°35'34''$	355.6157	5.4436	112	11	1131273	1.60
BLG364	$17^h13^m40.^s1$	$-32°00'03''$	353.6439	4.0516	112	13	1095239	1.80
BLG365	$17^h09^m30.^s0$	$-32°00'02''$	353.1234	4.7669	113	12	964653	1.58
BLG366	$17^h06^m29.^s9$	$-32°44'57''$	352.1412	4.8308	115	11	911721	1.51

frames is not strictly related to their typical observing frequency.

3. Photometric Maps of the Galactic Bulge Fields

3.1. Catalog

The construction of the general catalog – photometric map of the Galactic bulge was done similarly to the procedure applied to other main targets of the OGLE-III observations, the Magellanic Clouds and the Galactic disk. The procedure was detailed in Udalski *et al.* (2008b). Here, we only recall the main features and describe small changes.

The catalog tables were created for every subfield (chip nos. 1–8) separately. This is a logical consequence of the fact that images of each mosaic chip were considered as individual parts of every main field as listed in Table 1. The reference images, reductions and databases were also made separately for every subfield.

As it was mentioned above, about 7% of the total area covered in the Galactic bulge is overlapped by more than one field. Accordingly, a few percent of all objects can be found in more than one subfield catalog. The current, text version of the photometric maps does not provide cross-identification of those objects but we plan to include it in the online version of the database which will be available in near future.

The catalog was constructed based on the *I*-band databases. Adding the *V*-band photometry required cross-identification between objects in *I* and *V* databases. The matching star in *V* was chosen to be the closest object in $0\farcs5$ (1.9 pixel) radius. For objects identified in more than one (overlapping) subfield we were able to construct single *V* data sets of independent measurements for each star.

The data in the catalog tables include: star ID (column 1); equatorial coordinates J2000.0 (2,3); X,Y pixel coordinates in the *I*-band reference image (4,5); photometry data *V*, $V-I$ and *I* (6,7,8), *V*-band photometry parameters: number of points used for mean magnitude (9), number of 5σ-rejected points (10) and standard deviation σ (11); *I*-band photometry parameters, same as for *V* (12, 13, 14). Values of 9.999 and 99.999 mark no data available in the given column. Values prefixed with plus sign in column (10) indicate multiple *V*-band cross-identification. Table 2 presents a sample of catalog table for field BLG100.1.

The mean photometry was derived for all objects with minimum of 1 and 6 observations in the *V* and *I*-band, respectively, by averaging all observations after removing 5σ deviating points. The limit for *V* is so low because of the small overall number of *V*-band observations in bulge fields. In the case of stars that had been

T a b l e 2

OGLE-III Photometric Map of the BLG100.1 field (sample)

ID	RA (2000)	DEC (2000)	X	Y	V	$V-I$	I	N_V	$N_V^{\rm bad}$	σ_V	N_I	$N_I^{\rm bad}$	σ_I
1	$17^{\rm h}51^{\rm m}01^{\rm s}.01$	$-30^\circ16'16''.9$	389.87	17.04	19.583	5.371	14.212	6	0	0.049	1330	0	0.053
2	$17^{\rm h}51^{\rm m}01^{\rm s}.20$	$-30^\circ15'39''.4$	533.88	27.13	15.919	1.969	13.950	7	0	0.007	1547	4	0.015
3	$17^{\rm h}51^{\rm m}01^{\rm s}.60$	$-30^\circ16'17''.5$	387.42	46.62	13.684	0.824	12.860	6	1	0.002	1849	1	0.018
4	$17^{\rm h}51^{\rm m}01^{\rm s}.73$	$-30^\circ16'07''.6$	425.45	52.99	15.017	1.100	13.916	7	0	0.006	1915	0	0.014
5	$17^{\rm h}51^{\rm m}02^{\rm s}.25$	$-30^\circ16'15''.0$	396.82	78.91	99.999	9.999	14.807	0	0	9.999	1381	0	1.042
6	$17^{\rm h}51^{\rm m}02^{\rm s}.39$	$-30^\circ17'29''.8$	109.36	84.93	13.512	0.761	12.751	8	0	0.005	2147	0	0.017
7	$17^{\rm h}51^{\rm m}02^{\rm s}.47$	$-30^\circ15'45''.5$	510.54	89.89	14.610	1.132	13.479	8	0	0.002	2192	3	0.013
8	$17^{\rm h}51^{\rm m}03^{\rm s}.11$	$-30^\circ16'33''.5$	325.87	121.45	17.709	3.546	14.162	8	0	0.022	2307	0	0.013
9	$17^{\rm h}51^{\rm m}03^{\rm s}.79$	$-30^\circ16'57''.0$	235.10	154.61	17.066	3.359	13.708	8	0	0.007	2373	1	0.009
10	$17^{\rm h}51^{\rm m}03^{\rm s}.93$	$-30^\circ17'05''.3$	203.24	161.44	19.237	5.418	13.818	8	0	0.065	2380	0	0.081
11	$17^{\rm h}51^{\rm m}04^{\rm s}.71$	$-30^\circ16'18''.6$	382.82	201.19	19.248	4.728	14.520	8	0	0.048	2386	0	0.015
12	$17^{\rm h}51^{\rm m}05^{\rm s}.13$	$-30^\circ16'10''.9$	412.40	222.06	18.699	4.592	14.107	8	0	0.032	2385	1	0.009
13	$17^{\rm h}51^{\rm m}05^{\rm s}.47$	$-30^\circ17'19''.6$	148.21	237.78	14.309	1.732	12.577	8	0	0.006	2382	1	0.010
14	$17^{\rm h}51^{\rm m}05^{\rm s}.98$	$-30^\circ15'56''.2$	468.60	264.46	17.975	4.669	13.306	8	0	0.021	2387	0	0.043
15	$17^{\rm h}51^{\rm m}05^{\rm s}.99$	$-30^\circ15'37''.4$	541.07	265.11	14.553	1.294	13.259	8	0	0.002	2382	5	0.016
16	$17^{\rm h}51^{\rm m}06^{\rm s}.13$	$-30^\circ15'48''.3$	499.02	271.90	18.801	4.937	13.864	8	0	0.085	2387	0	0.038
17	$17^{\rm h}51^{\rm m}06^{\rm s}.21$	$-30^\circ16'13''.8$	401.11	275.78	14.912	0.840	14.072	7	1	0.003	2387	0	0.011
18	$17^{\rm h}51^{\rm m}06^{\rm s}.34$	$-30^\circ15'38''.4$	537.13	282.71	12.838	9.999	99.999	7	1	0.002	0	0	9.999
19	$17^{\rm h}51^{\rm m}07^{\rm s}.04$	$-30^\circ16'01''.1$	449.83	316.87	15.199	1.144	14.055	8	0	0.004	2386	1	0.012
20	$17^{\rm h}51^{\rm m}07^{\rm s}.20$	$-30^\circ17'08''.7$	189.55	323.89	17.192	3.975	13.216	8	0	0.069	2387	0	0.036
21	$17^{\rm h}51^{\rm m}07^{\rm s}.41$	$-30^\circ17'42''.2$	60.59	333.81	19.002	4.809	14.193	7	1	0.022	2026	2	0.022
22	$17^{\rm h}51^{\rm m}07^{\rm s}.58$	$-30^\circ16'48''.5$	267.43	343.34	14.695	0.929	13.766	7	1	0.003	2385	2	0.011
23	$17^{\rm h}51^{\rm m}08^{\rm s}.22$	$-30^\circ17'31''.7$	101.15	374.20	15.878	2.986	12.892	8	0	0.008	2334	10	0.007
24	$17^{\rm h}51^{\rm m}08^{\rm s}.48$	$-30^\circ17'10''.0$	184.32	387.71	16.824	3.591	13.233	8	0	0.009	2380	7	0.006
25	$17^{\rm h}51^{\rm m}08^{\rm s}.46$	$-30^\circ15'50''.3$	491.17	387.61	17.876	3.721	14.155	8	0	0.016	2381	6	0.008

identified in V-band on more than one subfield, all V observations formed a single data set and then were averaged because they are independent measurements. Finally, the color term correction was applied for each object to its database average magnitude according to the transformation equations and color term coefficients presented in Udalski *et al.* (2008a). The $(V-I)$ color derived from the database I and V values was converted to the standard system using $(V-I) = (v-i)/(1-\varepsilon_V+\varepsilon_I)$ formula. Then, V and I magnitudes were adjusted by adding $\varepsilon_{V,I} \cdot (V-I)$ term to the database value. For objects that do not have color information the average $(V-I)$ of the field was used for color correction of respective I or V magnitude. For other OGLE-III targets (Magellanic Clouds, Galactic disk) the mean value for the whole population was used but for the Galactic bulge the differences in mean $(V-I)$ are so big (see Table 1) that we decided to use proper mean values for each field. The "database" values mentioned here are the instrumental magnitudes corrected for subtle effects discussed in detail by Udalski *et al.* (2008a).

The catalog includes all objects which are present in the I-band databases. With the additional criteria for the quality of the photometry, described above, a small number of objects (less than 2%) entered the catalog with no photometry given, marked by 99.999 values in both I- and V-bands. For the sake of simplicity and to keep the star IDs consistent with the databases, we have not removed these objects from the catalog.

The astrometry was done in the same way as in previously published OGLE-III Photometric Maps, using third-order transformation based on 2MASS Catalog (Skrutskie *et al.* 2006). The details are given in Udalski *et al.* (2008a).

3.2. *Improved Calibration of Red Objects*

As it was mentioned above and discussed in earlier papers (Udalski *et al.* 2002), the original calibration of the OGLE-II and OGLE-III photometry was slightly inaccurate for very red or heavily reddened objects, especially in the Galactic bulge where the interstellar extinction is large. This was mainly due to the fact that the I-band filter used during the second and third phases of the project was different from the standard Kron-Cousins definition (Landolt 1992), exhibiting quite wide transparency "wing" into the infrared part of the spectrum. Furthermore, there are practically no standard stars with $(V-I) > 2$ mag because such red objects are usually variable. Thus, the OGLE-II and OGLE-III I-band filter photometry could not be calibrated precisely to the standard KC (Landolt) system for stars redder than $(V-I) > 2$ mag. Therefore extrapolated transformation coefficients derived from the observed standard stars in the $(V-I) < 2$ mag range had to be used. This may, however, lead to the systematic I-band deviations in the OGLE map I-band magnitudes, as shown in Fig. 2 of Udalski *et al.* (2002).

Since the beginning of the OGLE-IV phase in 2010, the project has been using the new, interference V- and I-band filters. OGLE-IV I-band filter very closely reproduces I-band definition adopted by Landoldt (1992) in his commonly used set of standard stars – the system to which the OGLE data are ultimately tied. We may assume that the OGLE-IV I-band filter can be practically considered the standard one.

When the first season of OGLE-IV observations was completed, we were able to compare and recalibrate OGLE-III photometry. To this end, we cross-identified a number of constant stars in selected OGLE-III and OGLE-IV Galactic bulge fields. We chose several highly reddened fields where the photometrically stable bulge red giants and disk main sequence stars are shifted to high $(V-I)$ colors of 3–6. In this way we obtained a huge set of photometric standards with extremely large $(V-I)$.

To double-check that OGLE-IV I-band filter can be indeed treated as the standard one we compared OGLE-IV photometry with OGLE-III photometric maps of selected LMC fields where the vast majority of stars are bluer than $(V-I) = 1.5$ mag. We found a constant shift of magnitudes of these two datasets without any noticeable trend with the $(V-I)$ color indicating that indeed OGLE-IV I-band filter approximates the standard one very well.

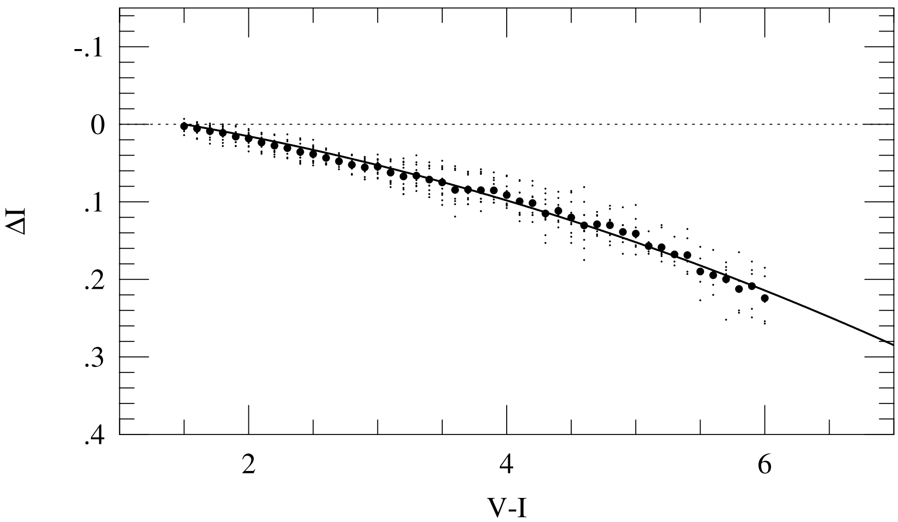

Fig. 2. I-band magnitude correction for red objects. Large dots show the mean values of differences taken from individual fields (small points). Solid line shows the parabola fitted to the mean values. Dotted line marks zero correction level for convenience.

To calibrate the OGLE-III photometry of redder objects we compared the mean magnitudes from OGLE-IV photometry and OGLE-III uncalibrated maps of the selected Galactic bulge fields. The mean magnitude difference at $(V-I) = 1.5$ mag was assumed as the zero point for a given field. In the next step we merged the data from all compared fields and derived a mean difference of OGLE-IV (standard) photometry and uncalibrated OGLE-III map magnitudes and as a function of $(V-I)$ color. A second order polynomial was fitted to this relation and used further as the calibration function (Fig. 2):

$$\Delta I = -0.033918 + 0.016361(V-I) + 0.004167(V-I)^2 \text{ [mag]}.$$

The correction value, ΔI, reaches 0.02 mag at $(V-I) = 2.15$ mag, 0.05 at 3.0, 0.1 at 4.0 and 0.2 at 6.0, respectively. We note that the correction is approximately two times smaller than predicted in Udalski *et al.* (2002).

Finally we used the derived relation for correction of *I*-band photometry and $(V-I)$ color (for all objects with $(V-I) > 1.5$ mag) of all OGLE-III maps including the already released maps of the LMC, SMC and Galactic disk. The computed ΔI was added to I magnitude and subtracted from $(V-I)$ color of every object in the catalog. We estimate that the corrected *I*-band magnitudes are accurate to 0.01–0.02 for $(V-I) < 6$ mag.

3.3. Summary and Data Presentation

The OGLE-III Photometric Maps of the Galactic bulge fields contain entries for about 340 million stars located in 267 OGLE-III fields. Figs. 3–5 show the typical accuracy of the OGLE-III Photometric Maps of these targets: standard deviation of magnitudes as a function of magnitude in the *V*- and *I*-band for the fields BLG205.2, BLG245.7 and BLG292.5 of relatively high, moderate and low stellar density, respectively.

The completeness of the photometry can be assessed from the histograms presented in Figs. 6–8 for the same fields as in Figs. 3–5. It reaches $I \approx 19$ mag and $V \approx 20.5$ mag. It is worth noting that a significant number of objects (43%) do not have *V* photometry. This is mainly due to the large reddening of the Galactic bulge objects which makes them undetectable on OGLE-III *V* frames. The small overall number of *V* observations is another reason.

Figs. 9–11 present color–magnitude diagrams (CMDs) constructed for a few selected subfields from different Galactic bulge fields observed by OGLE-III survey. Additionally, Fig. 12 shows the CMD of one of the most reddened OGLE-III fields, BLG179. It is located at $b = -1\overset{\circ}{.}7$ where the interstellar extinction starts rapidly increasing toward the Galactic plane, eventually obscuring the whole Galactic bulge background. The red giant branch and red clump in BLG179 field are, therefore, significantly smeared out and elongated toward fainter magnitudes and redder $(V-I)$. To emphasize the effect, this diagram is compiled from the data of all eight subfields.

4. Data Availability

The OGLE-III Photometric Maps of the Galactic bulge are available to the astronomical community from the OGLE Internet Archive:

http://ogle.astrouw.edu.pl
ftp://ftp.astrouw.edu.pl/ogle3/maps/blg/

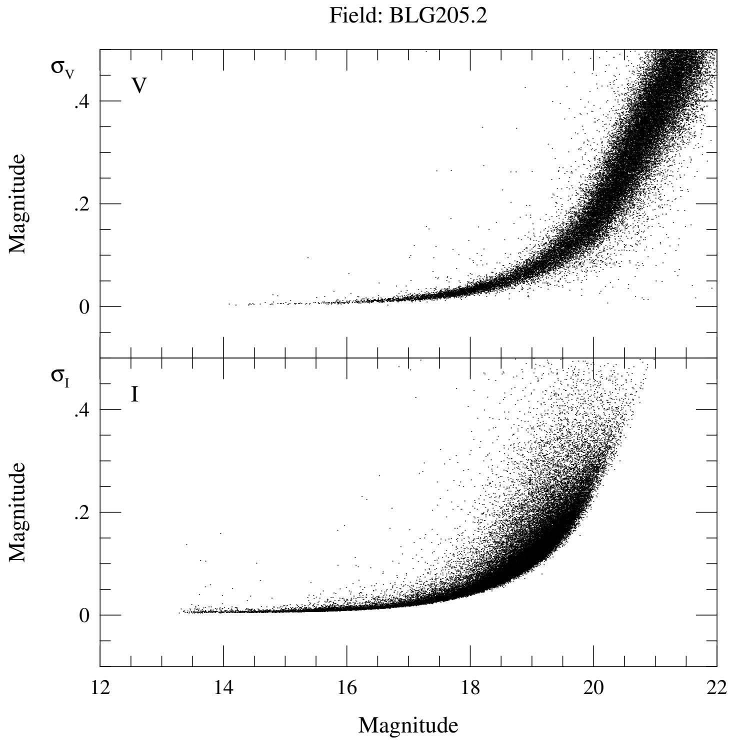

Fig. 3. Standard deviation of magnitudes as a function of magnitude for a high density BLG205.2 field

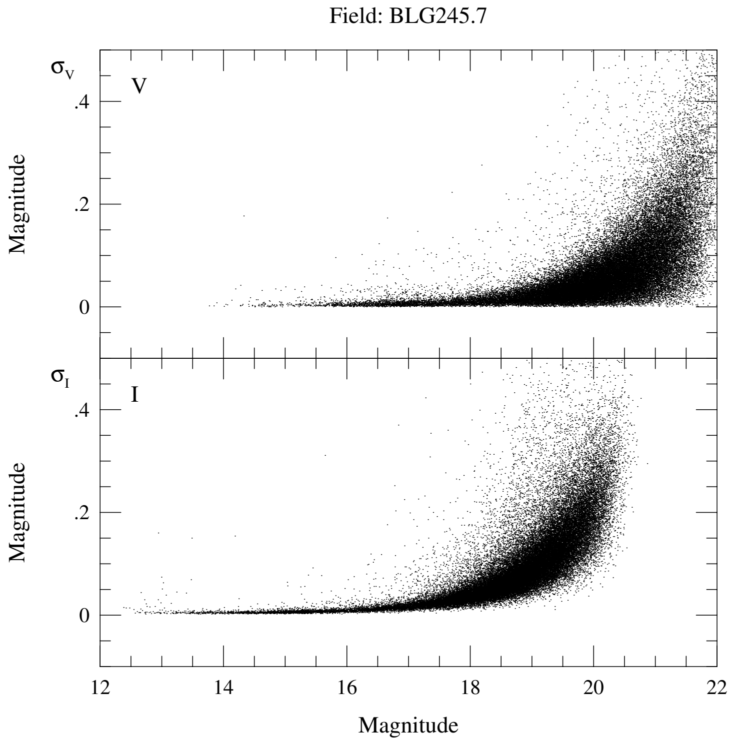

Fig. 4. Standard deviation of magnitudes as a function of magnitude for a moderate density BLG245.7 field

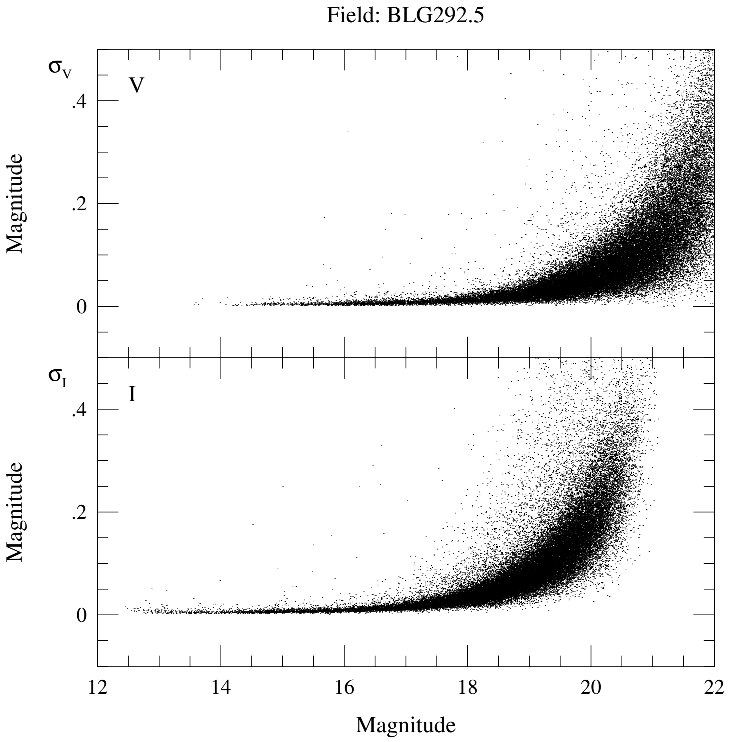

Fig. 5. Standard deviation of magnitudes as a function of magnitude for a low density BLG292.5 field

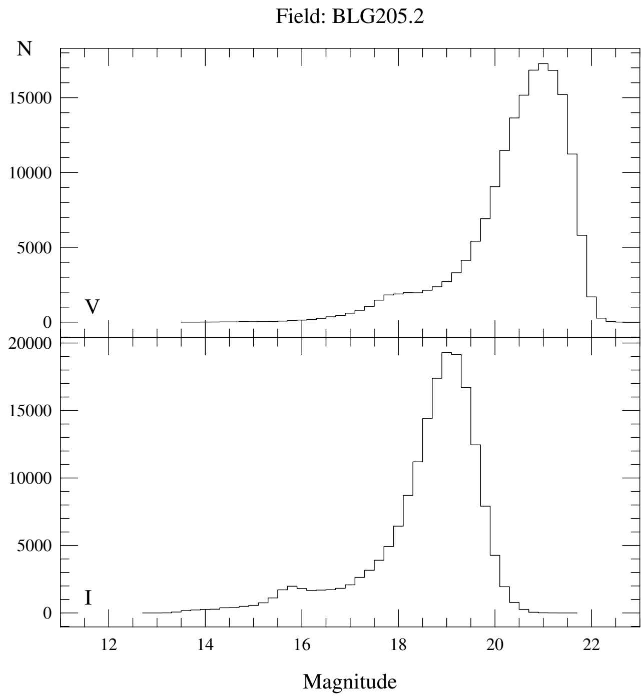

Fig. 6. Histogram of stellar magnitudes in the BLG205.2 field

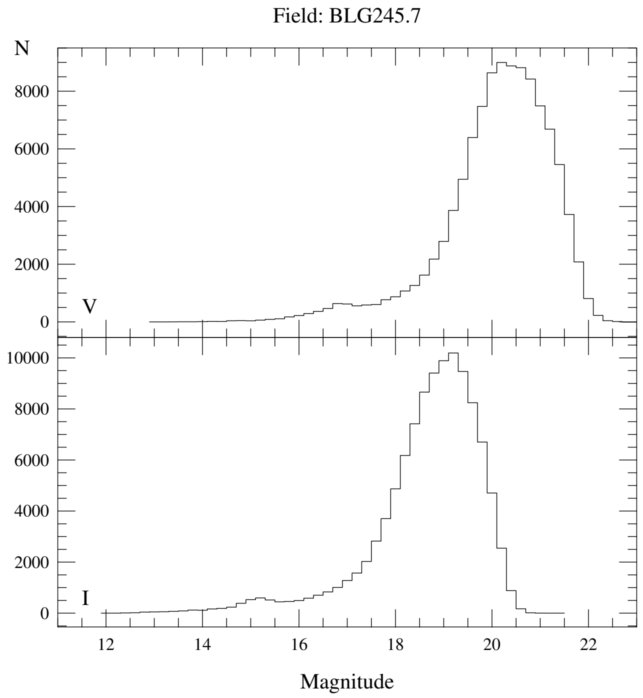

Fig. 7. Histogram of stellar magnitudes in the BLG245.7 field

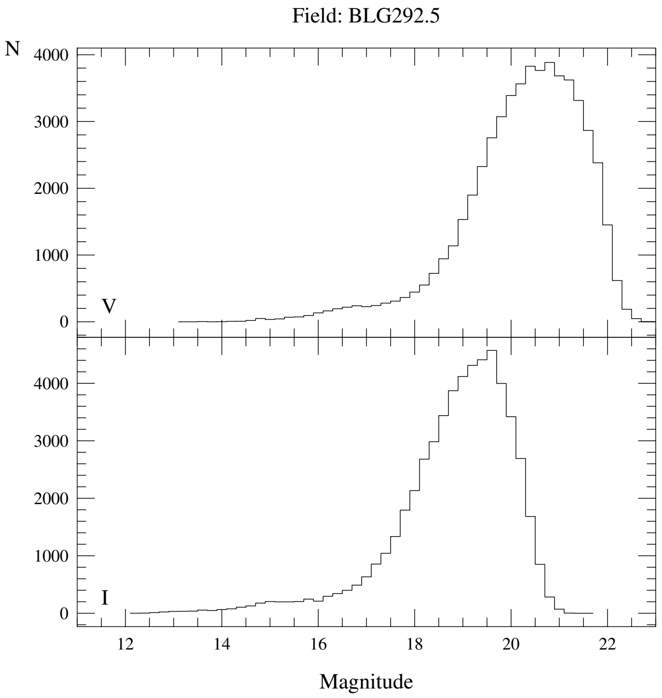

Fig. 8. Histogram of stellar magnitudes in the BLG292.5 field

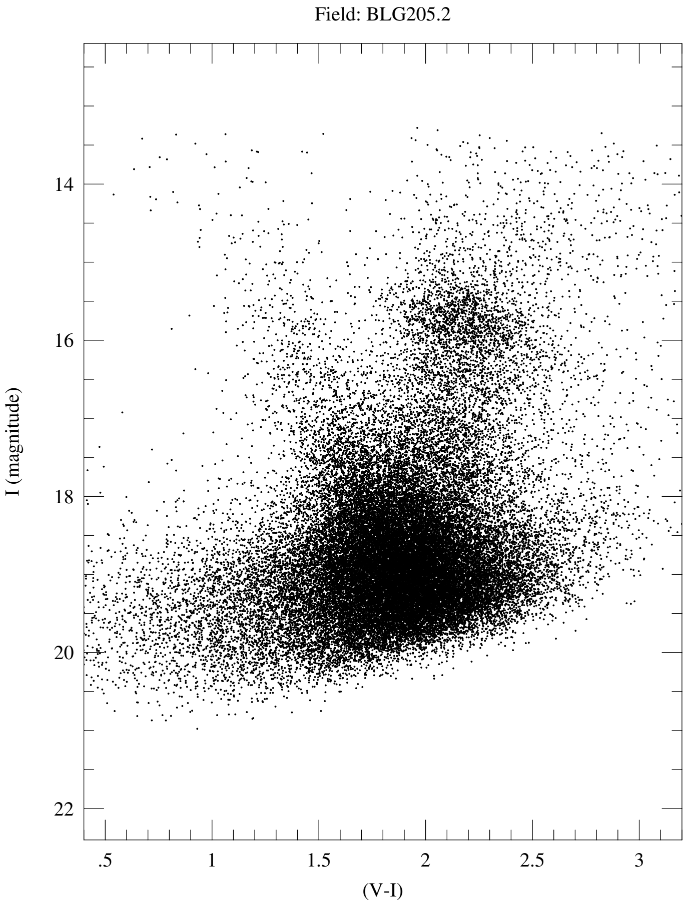

Fig. 9. Color–magnitude diagram of the BLG205.2 field.

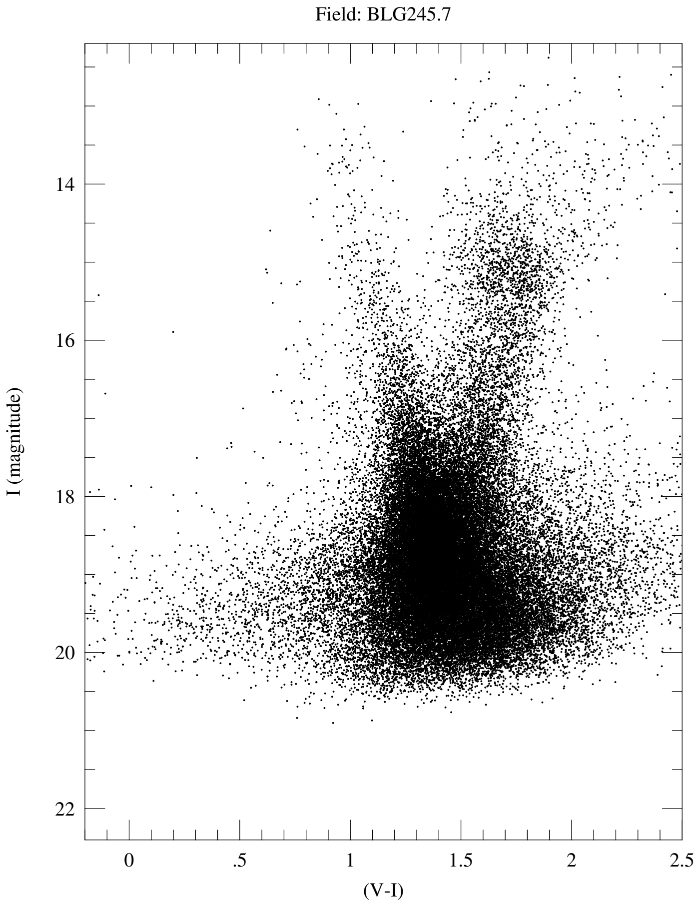

Fig. 10. Color–magnitude diagram of the BLG245.7 field.

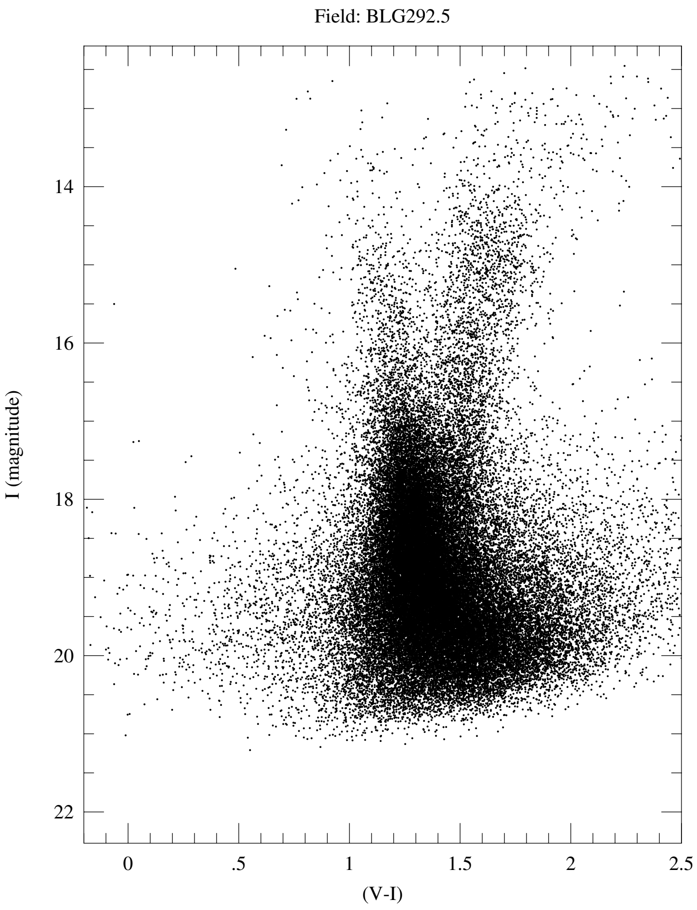

Fig. 11. Color–magnitude diagram of the BLG292.5 field.

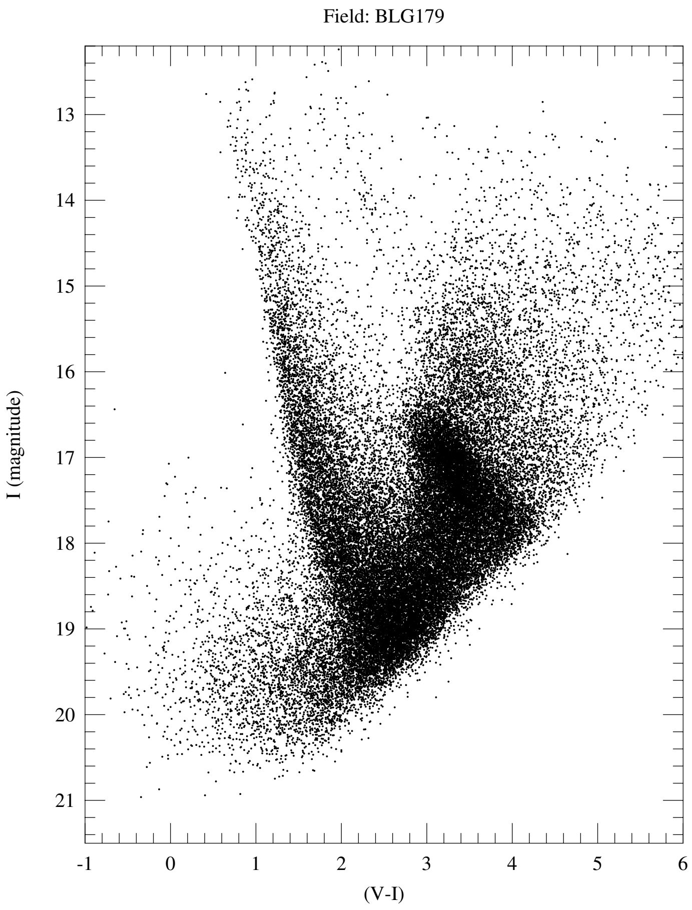

Fig. 12. Color–magnitude diagram of the highly reddened BLG179 field.

The archives include the catalog tables with photometric data and astrometry for each of the subfields. The *I*-band reference images are also available. The usage of the data is fully allowed for the general community. We only require the proper acknowledgment to the OGLE project.

We plan to build an online, interactive access to the photometric maps database, allowing to retrieve objects fulfilling a user-defined set of criteria. The availability of such an access will be announced on the OGLE project WWW page.

Acknowledgements. The OGLE project has received funding from the European Research Council under the European Community's Seventh Framework Programme (FP7/2007-2013) / ERC grant agreement no. 246678 to AU.

REFERENCES

Abe, F., *et al.* 2004, *Science*, **305**, 1264.
Bennett, D.P., *et al.* 2010, *Astrophys. J.*, **713**, 837.
Haschke, R., Grebel, E.K., and Duffau, S. 2011, *Astron. J.*, **141**, 158.
Landolt, A.U. 1992, *Astron. J.*, **104**, 372.
Nataf, D.M., Udalski, A., Gould, A., Fouqué, P., and Stanek, K.Z. 2010, *Astrophys. J.*, **721**, L28.
Rattenbury, N.J., Mao, S., Sumi, T., and Smith, M.C. 2007, *MNRAS*, **378**, 1064.
Skrutskie, M.F., *et al.* 2006, *Astron. J.*, **131**, 1163.
Subramaniam, A., and Subramanian, S. 2009, *Astrophys. J.*, **703L**, 37.
Szymański, M.K., Udalski, A., Soszyński, I., Kubiak, M., Pietrzyński, G., Poleski, R., Wyrzykowski, Ł., and Ulaczyk, K. 2010, *Acta Astron.*, **60**, 295.
Udalski, A., Szymański, M., Kubiak, M., Pietrzyński, G., Soszyński, I., Woźniak, P., Żebruń, K., Szewczyk, O., and Wyrzykowski, Ł. 2002, *Acta Astron.*, **52**, 217.
Udalski, A. 2003a, *Acta Astron.*, **53**, 291.
Udalski, A. 2003b, *Astrophys. J.*, **590**, 284.
Udalski, A., Szymański, M.K., Soszyński, I., and Poleski, R. 2008a, *Acta Astron.*, **58**, 69.
Udalski, A., Soszyński, I., Szymański, M.K., Kubiak, M., Pietrzyński, G., Wyrzykowski, Ł., Szewczyk, O., Ulaczyk, K., and Poleski, R. 2008b, *Acta Astron.*, **58**, 89.
Udalski, A., Soszyński, I., Szymański, M.K., Kubiak, M., Pietrzyński, G., Wyrzykowski, Ł., Szewczyk, O., Ulaczyk, K., and Poleski, R. 2008c, *Acta Astron.*, **58**, 329.